

Hydrodynamics of a Compound Drop in Plane Poiseuille Flow

Vignesh Thammanna Gurumurthy^{1, a)} and S. Pushpavanam^{1, b)}

Department of Chemical Engineering, Indian Institute of Technology Madras, Chennai-600036, India

(Dated: 6 December 2021)

We numerically investigate the hydrodynamics of a compound drop in a plane Poiseuille flow under Stokes regime. A neutrally buoyant, initially concentric compound drop is released into a fully developed flow, where it migrates to its equilibrium position. Based on the results, we find that the core-shell interaction affects the dynamics of both the core and the compound drop. During the initial transient period, the core revolves about the center of the compound drop due to the internal circulation inside the shell. At equilibrium, depending upon the nature of the flow field inside the shell, we identify two distinct core behaviors: stable state and limit-cycle state. In the stable state, the core stops revolving and moves outward very slowly. The core in the limit-cycle state continues to revolve in a nearly fixed orbit with no further inward motion. We also find that the migration of the compound drop affects the eccentricity of the core significantly. A comparison with the simple drop reveals that the core enhances the deformation of the compound drop. The outward moving core in stable state pushes the compound drop towards the walls, and the revolving core in limit-cycle state makes the compound drop to oscillate at its equilibrium position. From the parametric study, we find that the core affects the compound drop dynamics only at intermediate sizes, and increase in any parameter sufficiently causes a transition from limit-cycle state to stable state.

I. INTRODUCTION

A compound drop, also called a double emulsion, is a multicomponent liquid system consisting of one or more drops encapsulated inside another immiscible drop. The outermost drop is often referred as the shell and the inner ones as the core. The shell functions as a protective layer to the core from the ambient fluid. This feature makes the compound drops to be used as a delivery system, where the core can be loaded with chemical reactants^{1,2}, drugs³, and food additives⁴. In addition, it is also suited for in-situ culturing of cells and bacteria^{5,6}. Thus compound drops are highly desirable for applications related to bioanalysis, cosmetics, food and pharmaceutical industries.

Majority of the fundamental works on compound drops have focussed primarily on their production techniques and their dynamics in three basic flow geometries: (i) translation in a quiescent liquid^{7–10}, dynamics in (ii) extensional flows^{11–13} and (iii) linear shear flows^{11,14–19}. But, the pressure-driven flow (also known as Poiseuille flow) often encountered in microfluidic and biological flows has not been examined thoroughly yet. The stability of the compound drops moving in these flows play a huge role in applications related to targeted release of active ingredients in the core. Thus understanding the dynamics of compound drops in Poiseuille flow is crucial for the aforementioned applications.

Very few studies have investigated the dynamics of compound drops in Poiseuille flow^{20–24}, but they are not applicable at all conditions due to their underlying assumptions. The theoretical work by Song *et al.*²¹ studied the dynamics under Stokes regime in a capillary tube assuming both the shell and the core are perfectly spherical. Their analysis shows that the drag force on the core and the shell depends on vari-

ous parameters such as the viscosity ratio between the liquids (core-shell, shell-carrier), size ratio between the core and the shell, and eccentricity of the core. The use of perfectly spherical drop assumption limits their applicability since it is well known that the drops deform due to the confinement effects²⁵ which alters its shape. The numerical works by Zhou *et al.*²⁰ and Tau *et al.*²² investigated the morphological evolution of the compound drop moving in circular tube with a gradual contraction using phase field and boundary element methods respectively. Both studies show that the core affects the deformation of the compound drop and also prolongs the transit time in the contraction zone. Studies by Che *et al.*²⁴ and Borthakur *et al.*²³ simulated the dynamics of compound drop in axisymmetric microchannels using level-set and volume-of-fluid methods respectively. They investigated the temporal evolution of the drop shape, velocity fields, and the eccentricity of the core under the influence of parameters such as size of the compound drop, radius ratio, viscosity ratio and the capillary number.

The use of axisymmetry in the above studies limits their results to compound drops moving in circular microchannels. Even in circular channels, the axisymmetric configuration further constrains the axially moving drops (core and shell) to be at the centerline of the channel. But we know from theory of migration for simple drops²⁶ that only large drops, comparable to channel size, occupies the center, whereas smaller drops often migrate to an off-centered position. Recent experiments²⁷ have shown that the migration of compound drops in flow focusing geometries experience enhanced deformation. Thus, the effect of migration of the compound drop on the core, and the effect of core on the migration of the compound drop has not yet been understood clearly, and this forms the primary focus of this work.

In this work, we investigate the dynamics of the compound drop in a plane Poiseuille flow, which includes the migration and deformation dynamics of the core and the compound drop. The objectives of this study are to understand the (i) effect of migration of the compound drop on the dynamics of

^{a)}Electronic mail: vigneshgt@gmail.com

^{b)}Electronic mail: spush@iitm.ac.in

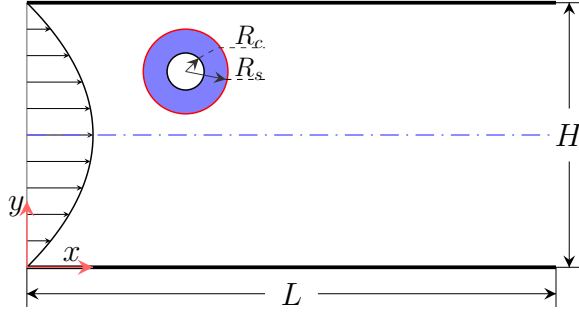


FIG. 1: Schematic of the computational domain. A neutrally buoyant, initially concentric compound drop is released into the fully developed flow.

the core, (ii) effect of core on the migration and deformation of the compound drop, and (iii) analyze the core-shell interaction under the influence of different parameters involved.

Rest of the paper is organized as follows. In section II we define the problem, list the governing equations and describe the numerical method adopted. In section III, we first describe the dynamics of the core followed by the compound drop, and finally the influence of different parameters on the equilibrium behaviors of the core and the compound drop. Finally, we summarize the results in section IV.

II. PROBLEM FORMULATION

A. Problem definition

Consider a concentric compound drop released in a fully developed plane Poiseuille flow as shown in the FIG 1. We choose the subscripts c , s , and d to denote the parameters related to the core, shell and the compound drop respectively. The radius of the undeformed core and shell are R_c and R_s respectively. We choose the commonly used core-shell-carrier fluid configuration in experiments: water-in-oil-in-water (W/O/W). This choice simplifies our problem to a two-phase flow since the core and the carrier phase are of the same liquid. The liquids are assumed to be Newtonian, and their densities are the same i.e, neutrally buoyant.

B. Governing equations

We model the two-phase flow using Volume-of-Fluid (VOF) method, a one-fluid formulation where the two immiscible fluids are treated as a one fluid. Since the flow rates associated with these systems are typically low, we neglect the convective term in the Navier-Stokes equations, but retain the unsteady acceleration term since we are also interested in the transient behavior. The governing equations under isothermal and incompressible flow conditions are,

$$\nabla \cdot \mathbf{U} = 0, \quad (1)$$

$$\rho \left(\frac{\partial \mathbf{U}}{\partial t} \right) = -\nabla P + \nabla \cdot (\mu \mathbf{D}) + \sigma \kappa \mathbf{n} \delta_s + \mathbf{S}_p, \quad (2)$$

where ρ , μ , \mathbf{U} and P represent density, viscosity, velocity and pressure field respectively. The deviatoric stress tensor \mathbf{D} is defined as $(\nabla \mathbf{U} + \nabla \mathbf{U}^T)$. The third term on the right hand side of equation (2) represents the surface tension force acting at the interface modelled as a body force term according to continuum surface force formulation²⁸. The use of Dirac delta function δ_s ensures that this force acts only in the vicinity of the interface and zero everywhere; Also, it acts along the interface normal \mathbf{n} . The symbols σ and κ denote the surface tension coefficient and curvature of the interface respectively. The flow through the channel is driven by a constant pressure gradient which is introduced as a source term \mathbf{S}_p in equation (2). It is given by,

$$\mathbf{S}_p = \frac{8\mu_c U_m}{H^2} \mathbf{i},$$

where U_m is the maximum velocity observed at the centerline of the channel and H is the channel height.

The two phases are distinguished by the scalar field f , which represents the volume fraction of the shell liquid. Computational cells with $f = 1$ represent the shell liquid and $f = 0$ represent either the core or the ambient liquid. Thus cells with f values between zero and one contain the interface whose motion is governed by the advection equation,

$$\frac{\partial f}{\partial t} + \nabla \cdot (f \mathbf{U}) = 0. \quad (3)$$

The viscosity is now defined as,

$$\mu = \mu_s f + (1 - f) \mu_c. \quad (4)$$

C. Non-dimensionalization

We non-dimensionalize the above equations (1)-(4) using the channel height H , centerline velocity U_m , and the ratio H^2/ν_c as the characteristic length, velocity, and time scale respectively. The characteristic time scale is the time needed for the momentum to diffuse across the channel, where ν_c is the kinematic viscosity of the ambient liquid. Pressure is scaled using the viscous friction given by $\mu_c U_m / H$, and the viscosity in equation (4) using μ_c . We write the non-dimensionalized equations in the same form as their dimensional counterparts for convenience, and they are given below,

$$\nabla \cdot \mathbf{U} = 0, \quad (5a)$$

$$\left(\frac{\partial \mathbf{U}}{\partial t} \right) = -\nabla P + \nabla \cdot (\mu \mathbf{D}) + \frac{\kappa \mathbf{n} \delta_s}{Ca} + 8, \quad (5b)$$

$$\frac{\partial f}{\partial t} + \nabla \cdot (f \mathbf{U}) = 0, \quad (5c)$$

where the viscosity is given by,

$$\mu = \mu_r f + (1 - f). \quad (5d)$$

In equation (5b), $Ca = \mu_c U_m / \sigma$ represents the capillary number which is the ratio between viscous and capillary forces. The symbol $\mu_r (= \mu_s / \mu_c)$ in equation (5d) represents the viscosity ratio between the two liquids. In addition to the above non-dimensional numbers, we also have radius ratio $K (= R_c / R_s)$ and aspect ratio $\lambda (= R_s / H)$ signifying the confinement effects of the shell on the core, and the wall on the shell respectively.

D. Numerical method

The above governing equations (5a)-(5c) are solved numerically using the open source code Basilisk^{29,30} written in C programming language. It uses a centered discretization for all scalar and vector fields. The equations (5a) and (5b) are solved using a pressure-projection approach, and the volume fraction field is advected using an operator-split algorithm. Bell-Collela-Glaz advection scheme³¹ is used for calculating the advective fluxes, and Runge-Kutta scheme for time advancement. All the discretizations are second-order accurate in space and time. The surface tension force in (5b) is accurately calculated using balanced force algorithm³², and the curvature of the interface is computed from the volume fraction field using height functions technique^{30,33}.

Basilisk provides an adaptive mesh refinement feature, which is used for refining specific regions for improving accuracy. The refinement is based on a wavelet transform of a given scalar field, which is used to assess its discretization error. The grid is locally refined if the calculated error is above the user-specified threshold and coarsened otherwise. In our simulations, we set the threshold refinement criteria for the scalar fields u , v (velocity fields) and f as 1×10^{-3} , 1×10^{-3} and 1×10^{-2} respectively. These values ensure that the regions close to the interfaces are sufficiently resolved, which is required for accurate calculation of the surface tension force.

E. Computational domain and boundary conditions

As often reported in the literature³⁴⁻³⁶, simulating cross-flow migration of a drop is time consuming because the rate of migration is inversely proportional to the deformation of the drop. Thus, it takes longer time for the drop to reach its equilibrium location. Hence, we restrict our investigations to two dimensions. Nevertheless, previous works^{34,35} have shown that the 2D simulations qualitatively captures the flow field obtained in the center plane of 3D simulations. Also, there is a good quantitative agreement for the equilibrium position of the drop calculated between the 2D simulations and the experiments^{34,35}.

The computational domain, as shown in the FIG. 1 is a rectangular domain of size $L \times H$. No slip and no penetration boundary conditions are enforced at the top and bottom

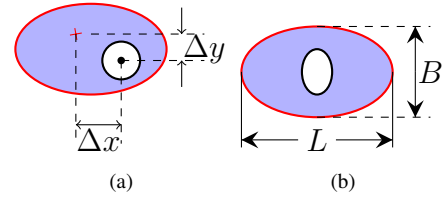


FIG. 2: Schematics showing the (a) definition of the eccentricity of the core and (b) measurement of deformation of the compound drop.

walls, and a periodic boundary condition at the right. The size ($L \times H$) of the computational domain is chosen as 2×1 for smaller drops ($\lambda \leq 0.2$) and 4×1 for larger drops. These different domain lengths for different drop sizes are chosen such that the drop-drop interaction due to periodicity is negligible.

We characterize the dynamics of the compound drop, and the core by studying their migration and deformation behavior. The migration of the compound drop is characterized by its transverse location y_d (centroid) measured from the bottom wall. In case of the core, we report its eccentricity, which is defined as $\Delta \vec{x} = \vec{x}_c - \vec{x}_d$, where \vec{x}_d , \vec{x}_c are the centroids of the compound drop and the core (see FIG. 2a). The deformation characteristics of the core and the compound drop are quantified by calculating the deformation parameter \mathcal{D} proposed by Taylor³⁷, which is defined as $\mathcal{D} = (\mathcal{L} - \mathcal{B}) / (\mathcal{L} + \mathcal{B})$. Here, \mathcal{L} and \mathcal{B} denote the length of the major and minor axis of the deformed droplet as shown in FIG. 2b. Each simulation is stopped shortly after equilibrium is reached i.e., when the parameters measured either attain a constant value or enter a periodic state.

Based on grid convergence tests (see appendix A), the size of the smallest region resolved in our simulations is 1.95×10^{-3} . We also have validated the solver with the experiments and the simulations reported in the literature on simple drops released in pressure-driven flows (see appendix B).

III. RESULTS AND DISCUSSIONS

A. Dynamics of the core

1. Distinct core behaviors

The temporal evolution of the eccentricity of the core is shown in FIG. 3a and FIG. 3b under two different conditions: (i) $Ca = 1$ and (ii) $Ca = 0.05$. Initially, under both conditions, we observe oscillations in the eccentricity in both directions. Eventhough they are slightly out of phase of with each other, their magnitudes are nearly the same. In the first case, the oscillations decay at a faster rate, eventually reaching a constant value. We call this equilibrium behavior as stable state. The oscillations in the second case decay slightly and enters a periodic state at long-times where it continues to oscillate at constant amplitude. We refer this periodic behavior as limit-cycle state. Thus at equilibrium, we observe two distinct behaviors,

which have also been observed for compound drops in linear shear flows^{17,18,38}.

The oscillations of the core observed in both directions indicate that it revolves inside the shell around the centroid of the compound drop, as illustrated in FIG. 3c and FIG. 3d. The core, as it revolves also moves inward in both cases. This revolving motion is due to the internal circulation inside the shell³⁹, which is the result of shearing of the shell interface due to the difference in velocities between the drop and the carrier fluid. The anticlockwise motion of the core and the internal circulation (see FIG. 4b & FIG. 4d) further supports the statement that the core revolves due to the circulation.

In the stable state, the core revolves in a circular orbit, and its radius reduces in each cycle in the same fashion similar to the decay of oscillations observed in FIG. 3a. As shown in the inset in FIG. 3c, at equilibrium the core stops revolving but starts translating upwards. The cross-stream distance travelled due to this motion is very small. The core in the limit-cycle state, also starts revolving and moving inward initially. But at equilibrium, it enters into an egg shaped orbit (see FIG. 3d), where its length in each cycle remains nearly the same thereafter, and also, it does not move inward any further.

2. Underlying mechanism

The two distinct core behaviors at equilibrium can be explained by analysing the rotational flow field they experience inside the shell. The velocity field in any incompressible flow can be decomposed into strain rate tensor and vorticity tensor responsible for deformation and rigid-body rotation respectively. A drop in pure straining field will undergo planar extension resulting in stretching and compressing along the principal axes. The same drop would simply rotate in a pure vorticity field, while retaining its initial (spherical) shape and aligning itself along the symmetry axis⁴⁰. In a linear shear flow, where these two components are in equal proportion, the drop would stretch linearly in time and tilt toward the flow direction⁴¹.

In the Poiseuille flow simulated here, we identify the magnitude of strain rate tensor from the deformation of the core, and the vorticity tensor from the local vorticity field. From FIG. 4b and FIG. 4d, we see that the magnitude of the vorticity field in limit-cycle state is higher than in the stable state. The prolate ellipsoid and the circular shapes of the core in the FIG. 4b and FIG. 4d clearly show that the deformation is higher in the stable state. This qualitative conclusion is supported by the quantitative measurements of the deformation shown in FIG. 6a and FIG. 6b, where we observe that the deformation parameter \mathcal{D} of the core in stable state is one order of magnitude higher than the limit-cycle state. Thus, large deformation and small vorticity field experienced by the core in stable state shows that the strain rate tensor is dominant. This dominant strain rate tensor aligns the core along the principal axes (see FIG. 4b) thereby arresting its revolution, and also results in its very slow outward motion. The dominant vorticity field in the limit-cycle state causes the core to revolve in a nearly fixed orbit which resembles rigid-body rotation. It also

causes orientation of the core to oscillate as shown in FIG. 5.

3. Deformation dynamics

As the core revolves, it comes closer to the shell interface in each cycle. At this instant, the liquid in the gap between the two interfaces gets squeezed causing a pressure buildup. This pressure buildup affects the deformation of the core every time it comes near the shell interface, and decreases in each cycle due to increase in the thickness of the gap as the core moves inward. Thus, the deformation of the core characterized by the deformation parameter \mathcal{D} oscillates as seen in FIG. 6a and FIG. 6b. These oscillations in the case of a stable state decay with time, and reaches a constant value once the core stops revolving. The deformation of the core in the limit-cycle state continues to oscillate due to its revolving motion. The kinks (point C in FIG. 6b) observed in \mathcal{D} at each cycle are due to the slightly out of phase nature of the oscillations of the core. As shown in FIG. 3b, the core reaches its maximum in both directions one after the other which in turn affect their deformation thereby resulting in the kinks. Similar trends have also been reported in temporal evolution of the deformation of the simple drop in Poiseuille flows under Stokes conditions⁴².

B. Dynamics of the compound drop

1. Deformation

The temporal evolution of the deformation parameter \mathcal{D} of the compound drop in the two states are shown in FIG. 6a and FIG. 6b. It follows the same trend as the core in both states. The parameter \mathcal{D} oscillates initially, which later attains a constant value in the case of stable state, whereas it continues to oscillate in the limit-cycle state. By comparing the core positions (A – E) in FIG. 3b with the corresponding values in \mathcal{D} in FIG. 6b, we see that \mathcal{D} decreases when the core is closer to the shell and increases when it is far away.

The oscillations observed in \mathcal{D} occur due to the revolving motion of the core. As explained in the previous section, there is a pressure buildup in the gap between the core and the shell in each cycle when the core comes closest to the shell. This pressure buildup results in stretching of the shell which then relaxes as the core moves away from the shell. This cycle of stretching and relaxing of the shell resembles breathing, which has also been reported for compound drops in linear shear flows^{17,18,38}.

The effect of core on the compound drop is evaluated by comparing the temporal evolution of \mathcal{D} between the simple and the compound drop in FIG. 6a and FIG. 6b. The deformation of the simple drop is smaller than the compound drop, and also it does not oscillate during its evolution. We also observe that the compound drop in stable state deforms to an egg shape whereas the simple drop deforms to a parachute shape (see FIG. 4a and FIG. 4b). Since the compound drop in the limit-cycle state and the simple drop are subjected to low deformation ($Ca = 0.05$), they retain their initial circular

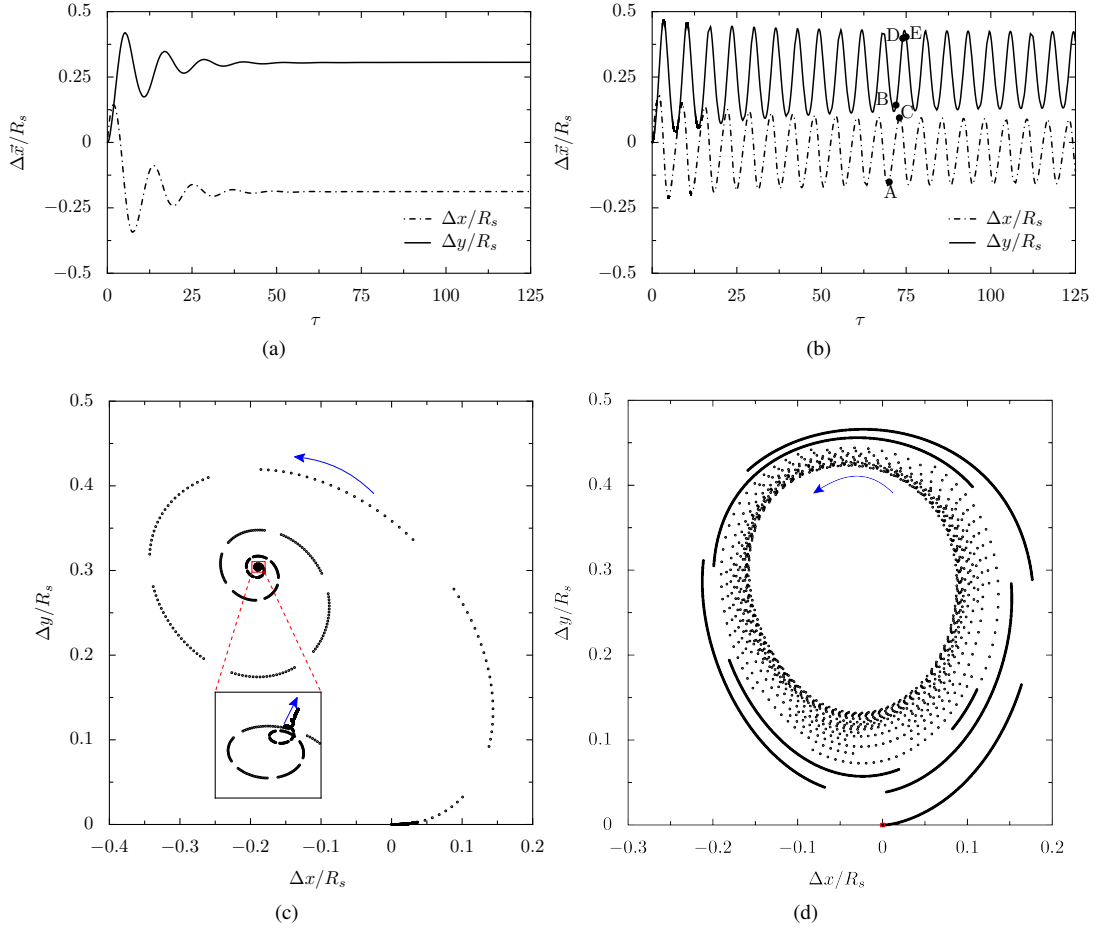


FIG. 3: Temporal evolution of the eccentricity of the core under (a) stable state and (b) limit-cycle state. Trajectory of the core inside the shell under (c) stable state and (d) limit-cycle state. The gaps seen in the trajectory of the core are due to the data ignored due to periodicity. The eccentricity of the core is measured relative to the centroid of the compound drop ($\Delta \vec{x} = \vec{x}_c - \vec{x}_d$). The common parameters between the two states are $AR = 0.2$, $k = 0.5$, $\mu_r = 1$ and the differing parameter is Ca which was kept at $Ca = 1$ for the stable state and $Ca = 0.05$ for the limit-cycle state.

shape. The orientation of the drop measured along the major axis for both simple and compound drop in both states are in the same direction along the principal axes. Thus from the above comparison with the simple drop, we find that the presence of core enhances the deformation of the compound drop and also causes the breathing motion.

We also observe from FIG. 6a and FIG. 6b that the deformation of the compound drop is larger in the stable state compared to the limit-cycle state since Ca is significantly larger in the stable state. Since the capillary force is inversely proportional to the drop size, the deformation of the compound drop is always higher than the core.

2. Migration

In a non-inertial flow, the cross flow migration of the drop occurs due to its deformation. This deformation occurs either due to the hydrodynamics of the flow or due to the con-

finement effects from the wall or both. The direction of migration due to this deformation induced lift force is either towards the center or the wall. It has been shown theoretically⁴³ that the drop migrates towards the wall if $1 \leq \mu_r < 10$, and towards the center otherwise. These theoretical predictions have been confirmed by experiments^{35,44} and simulations^{34,36}. They also have reported that the drops ($\lambda < 0.2$) migrate towards the center with increase in Ca . The above results only apply to smaller drops ($\lambda < 0.3$), the confinement effects from the walls always push larger drops ($\lambda \geq 0.3$) to the center.

We quantify the migration of the compound drop by measuring its vertical displacement from the bottom wall. The temporal evolution of migration of the compound drop and the simple drop are shown in FIG. 6c and FIG. 6d. The direction of migration of the compound drop and the simple drop are the same. These trends agree with the observations reported in literature for the simple drop, which were described above. When compared to a simple drop, the compound drop oscillates as it migrates. These oscillations are markedly noticeable

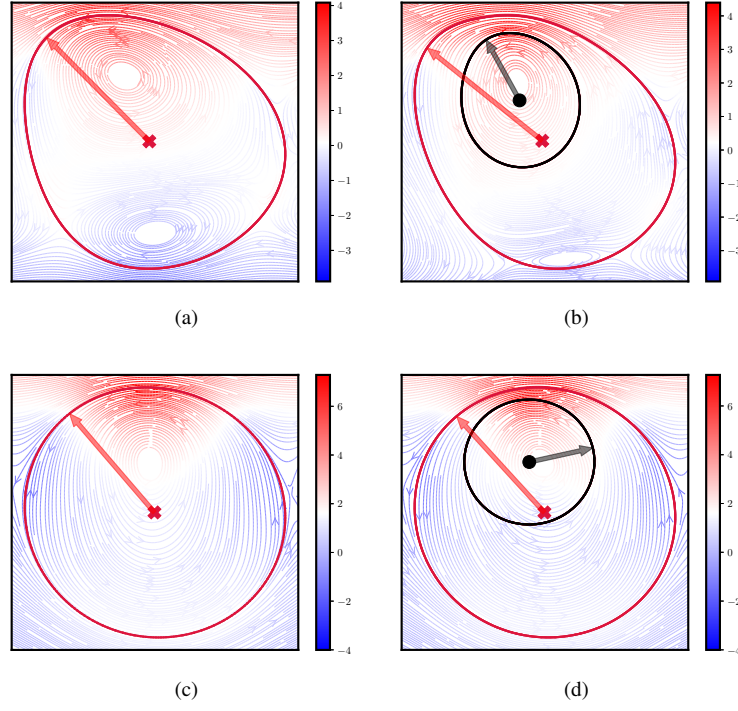


FIG. 4: Comparison of streamlines between simple drop and compound drop at equilibrium: (a) Simple drop (b) Compound drop in stable state (c) Simple drop (d) Compound drop in limit-cycle state. The streamlines are colored by the vorticity whose magnitude is shown in the colorbar. The red cross marker indicates the centroid of the simple and compound drop. The red arrow represents the orientation of the simple and the compound drop measured along the major axis. Similarly the black dot and the black arrow indicate the centroid and the orientation of the core. The orientation is measured along the major axis \mathcal{L} . The parameters used are the same as shown in FIG. 3.

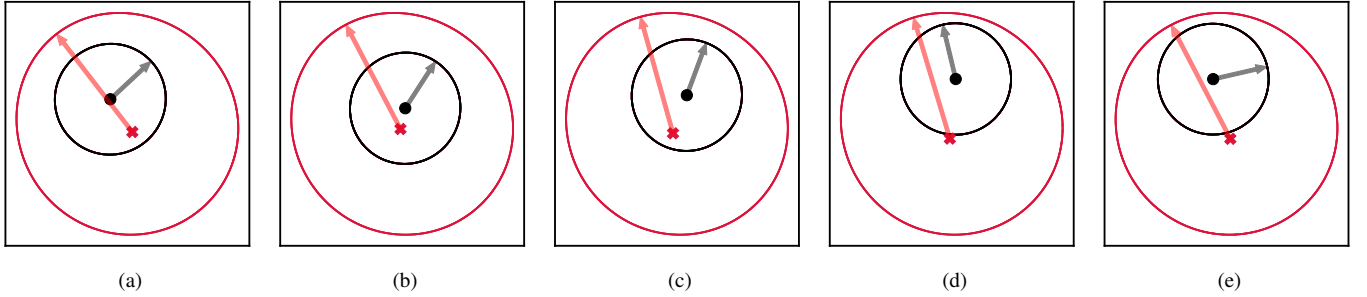


FIG. 5: Revolving motion of the core in limit-cycle state. Figures (a)-(e) represent the position of the core inside the shell at points A-E in FIG. 3b. The red cross marker and the red arrow indicate the centroid and the orientation of the compound drop. Similarly the black dot and the black arrow indicate the centroid and the orientation of the core. The orientation is measured along the major axis \mathcal{L} .

in the limit-cycle state than in the stable state. Both the motion of the compound drop and the core are synchronized. By comparing the core positions marked by the points B, D, E in FIG. 3b and the corresponding location of the drop in FIG. 6d, we see that they reach their maximum and minimum heights together in each cycle. This synchronized motion is a result of the core pushing the shell upward as it reaches its peak in each cycle. Similar oscillatory motion due to the core has been ob-

served experimentally in self propelling encapsulated nematic shells⁴⁵.

The equilibrium position of the compound drop is slightly higher than the simple drop in the stable state whereas we observe a reverse scenario in the limit-cycle state. The slight upward motion of the core after it stops revolving in the stable state pushes the shell resulting in slightly higher position of the compound drop. The continued revolution of the core in

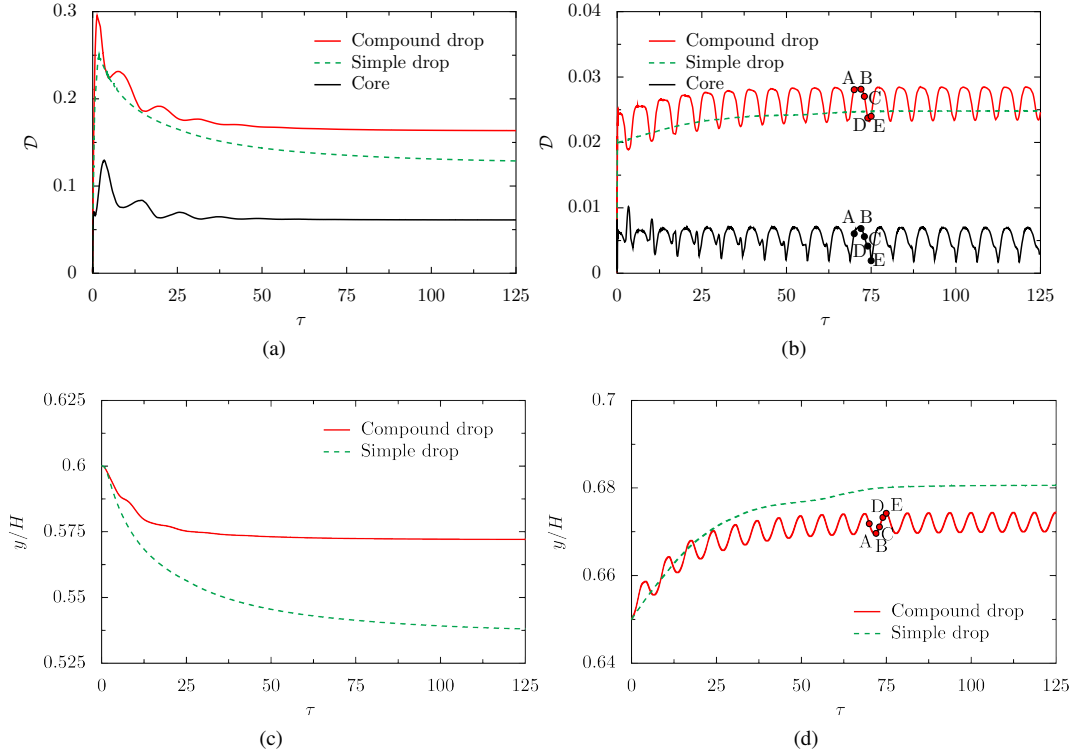


FIG. 6: Temporal evolution of the deformation compound drop under (a) stable state and (b) limit-cycle state. Temporal evolution of the height of the compound drop measured from the bottom wall under (c) stable state and (d) limit-cycle state. The parameters used for the two states were the same as in the FIG. 3.

the limit-cycle state only makes the compound drop to oscillate. Thus, the presence of core affects the migration of the compound drop.

The change in the equilibrium position of the compound drop due to the core also affects the circulation pattern inside the shell. From FIG. 4a and FIG. 4b, we see that the circulation observed in the bottom half of the simple drop reduces significantly in the compound drop due to its slightly higher position. We know that the circulation is the result of shearing of the shell interface due to the difference in velocities between the interface and the surrounding fluid. Due to its position, a major part of the simple drop lies in the upper-half, and the rest lies in bottom-half of the channel, which leads to the interface being sheared in opposite directions unequally resulting in the two circulation patterns. The slight increase in the height of the compound drop leaves only a small portion of the shell interface exposed to shear in the bottom-half of the channel, thereby modifying the circulation pattern inside the shell. Since the compound drop in the limit-cycle state and its equivalent simple drop are completely in the upper-half of the channel, we observe from FIG. 4c and FIG. 4d only a slight shift in the center of the circulation.

The migration of the compound drop also influences the position of the core i.e., eccentricity. Different core configurations due to the migration of the compound drop are shown in FIG. 7. The parameters used for the different configurations and the corresponding equilibrium positions are listed in

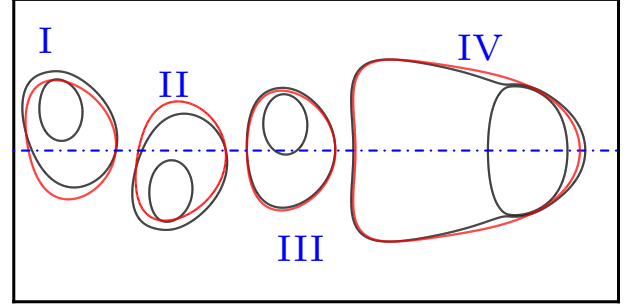


FIG. 7: Effect of migration of the compound drop on the core position. The interface shapes shown in red and black colours represent the simple and compound drops respectively. The blue dash-dotted line is the centerline of the channel. The parameters used for these cases are given in the Table I.

the Table I. The eccentric positions of the core shown in FIG. 7 are often observed in experiments^{5,39,46,47}. It is well known that for a drop moving in a channel (2D) two equilibrium locations exists on either side of the centerline. The position of the core switches to opposite sides depending upon these two positions, but always closer to the wall. The core becomes symmetric about the centerline only when the compound drop is also at the center. Also, in this symmetric position, the core occupies the front of the shell, which is the only configuration

Index	λ	μ_r	y_{eq}/H	
			Simple	Compound ¹
I	0.2	1	0.537	0.572 ²
II	0.2	1	0.464	0.427 ²
III	0.2	0.1	0.5	0.509
IV	0.4	1	0.5	0.5

¹ $K = 0.5$ was set for all the compound drops.

² Initial release heights for drops I and II are 0.6 and 0.4 respectively.

$Ca = 1$ was used for all simulations.

TABLE I: Parameters used for cases shown in FIG. 7.

reported in the axisymmetric simulations^{20–24}. Even though the equilibrium position of the drop *III* in FIG. 7 is very close to the centerline, the core occupies an asymmetric location.

The concentric drop configuration used as initial condition in our simulations is rarely realized in experiments. Thus, we studied the effect of initial eccentricity of the core on the migration and deformation dynamics of the core and the compound drop (see supplementary information). In addition, we also studied the effect of the initial release height of the drop. Based on the results, we find that the variation of the initial conditions only affect the initial transients, while their equilibrium behavior remains the same.

C. Core-shell interaction

From the results discussed above, we find that the core and shell interact through the fluid inside the shell as follows. The compound drop deforms due to the ambient flow conditions inside the channel, and the resulting deformation induced lift force causes the compound drop to migrate. The deformation of the shell by shearing also causes the fluid inside it to circulate, which makes the core to revolve. The intensity of deformation of the shell interface also affects the rotational flow field inside the shell which in turn determines the equilibrium core behavior. We also saw that direction of migration of the compound drop also affects the position of the core inside the shell. Thus the shell influences the core behavior by altering the flow field inside the shell. By comparing with the simple drop, we find that the core in these two states enhances the deformation of the compound drop. In addition, the core in the stable state pushes the compound drop slightly towards the wall, while the core in the limit-cycle state causes the compound drop to oscillate at equilibrium. We further note that the two different core behaviors and their effects on the compound drop dynamics were illustrated at two different capillary numbers ($Ca = 0.05$ and $Ca = 1$) which clearly indicates that the ambient flow conditions dictate the interaction.

D. Parametric Study

In this section, we investigate the influence of each parameter on the core-shell interaction and their effects on the core and the compound drop dynamics. Since the transient dynamics depend strongly on the initial conditions, we only report the equilibrium behavior. We represent the oscillating behavior of limit-cycle state cases by taking its average with error bars representing its maximum and minimum values.

1. Effect of viscosity ratio and capillary number

The deformation of the compound drop characterized by the parameter \mathcal{D} are shown in FIG. 8a and FIG. 9a for varying viscosity ratio and capillary number respectively. As expected, similar to the simple drop, the deformation of the compound drop also increases with increasing μ_r and Ca . The presence of core enhances the deformation of the compound drop, thus it is always higher than the simple drop except at low Ca , where it is nearly the same as the simple drop. The deformation of the core also follows the same increasing trend with μ_r and Ca . Thus, we observe a transition from limit-cycle state to stable state with increase in either μ_r or Ca .

The variation of the equilibrium position of the compound drop with μ_r and Ca are shown in FIG. 8b and FIG. 9b. These trends agrees with the reported observations made for the simple drop discussed in the previous section. The equilibrium position of the compound drop is always higher than the simple drop in the range of μ_r studied, but only at higher values of Ca . At low Ca , the equilibrium position of the simple drop is slightly higher than the compound drop due to the revolving core in the limit-cycle state.

The eccentricity of the core, as shown in FIG. 8c, oscillates with increasing μ_r (increasing first and then decreasing). The eccentricity of the core (see FIG. 9c) in the vertical direction increases with Ca and attains a constant value quickly, while in horizontal direction it decreases with increase in Ca . These trends in the eccentricity can be understood from the perspective of migration of the compound drop. When the drops are off-centered, the core occupies the backward part of the shell either at the top (see drop *I* in FIG. 7) or bottom (see drop *II* in FIG. 7) of the shell depending upon the equilibrium position of the drop. As the drop moves closer to the center, the core moves forward without changing its height (see drop *III* in FIG. 7). Similarly, the core moves backwards when the compound drop moves towards the walls.

2. Effect of aspect ratio

The deformation of the compound drop, as shown in FIG. 10a, increases with the drop size due to the additional deformation from the confinement effects due to the walls. The deformation of the compound drop is higher than the simple drop. The deformation of the core also increases with λ but decreases slightly once the compound drop is at the center, which happens when $\lambda \geq 0.3$. This reduction in deformation

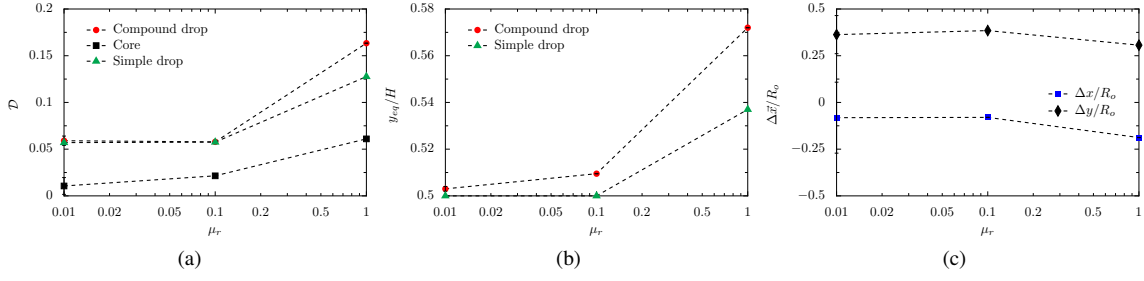


FIG. 8: Effect of viscosity ratio on the (a) deformation of the compound drop and the core, (b) migration of the compound drop, and (c) eccentricity of the core at equilibrium. Other parameters were kept fixed at $\lambda = 0.2$, $K = 0.5$, and $Ca = 1$.

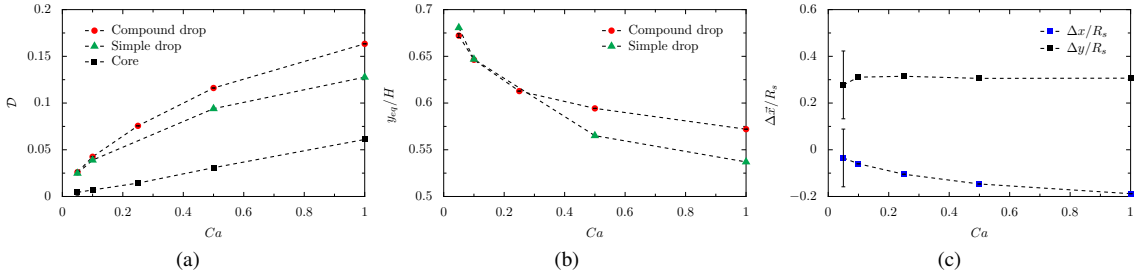


FIG. 9: Effect of capillary number on the (a) deformation of the compound drop and the core, (b) migration of the compound drop, and (c) eccentricity of the core at equilibrium. Other parameters were kept fixed at $\lambda = 0.2$, $K = 0.5$, and $\mu_r = 1$.

of the core is probably due to its position at the apex of the shell (see drop IV in FIG. 7), and has also been reported in axisymmetric compound drop moving in a circular pipe²⁴. We observed only stable state behavior in the entire range studied since Ca was kept at 1, which indicates large deformation. At lower Ca , we expect limit-cycle state in smaller drops which deforms less compared to large drops subjected to the same conditions.

The variation of equilibrium position of the compound drop with its size is shown in FIG. 10b. It clearly shows that the compound drop like the simple drop moves towards the center with increase in size. The simple drop reaches center when $\lambda \geq 0.3$, but the compound drop reaches the center only when $\lambda > 0.3$. This increase in threshold size for reaching the center is due to the presence of the core which pushes the compound drop towards the wall.

The variation of eccentricity of the core with λ is shown in FIG. 10c. The eccentricity in the vertical direction initially increases with λ , but reaches zero when the compound drop is in the center. Similarly, the eccentricity in horizontal direction initially decreases and starts increasing reaching its maximum when the compound drop is at the center. As long as the compound drop is off-centered and moves increasingly towards the wall, the core would move up and slightly backwards in the shell which explains the observed trend in eccentricity.

3. Effect of radius ratio

The deformation of the compound drop increases with increase in core size, as shown in FIG. 11a. But when the core size is either small or comparable to the compound drop ($K \geq 0.7$), its deformation decreases and becomes equal to the simple drop. This reduction in \mathcal{D} is due to the increased interaction between the core and shell^{24,48} at large K and very low interaction¹⁶ at small K . Such decreasing trends have also been observed for compound drops moving in circular pipes²⁴ and in shear flows^{17,18}. The deformation of the core, however, increases monotonically with its size due to the decrease in the capillary force. Thus, we observe a transition from limit-cycle to stable state behaviors with increase in core size.

The equilibrium position of the compound drop increases with the core size as seen in FIG. 11b, which indicates that the drop moves increasingly towards the wall. This behavior with core size confirms that the presence of core pushes the compound drop towards the wall. The equilibrium position is slightly lower than the simple drop when the core size is smallest due to its limit-cycle behavior.

From FIG. 11c, we observe that the eccentricity of the core decreases in vertical direction and increases in horizontal direction with K . As the core becomes larger it moves towards the center since it occupies larger space inside the cell which explains the observed trend in eccentricity.

Based on the simulations, we have constructed a regime diagram by varying the radius ratio and the capillary number while keeping the λ and μ_r fixed at 0.2 and 1 respectively. From FIG. 12, we observe that the threshold Ca above which

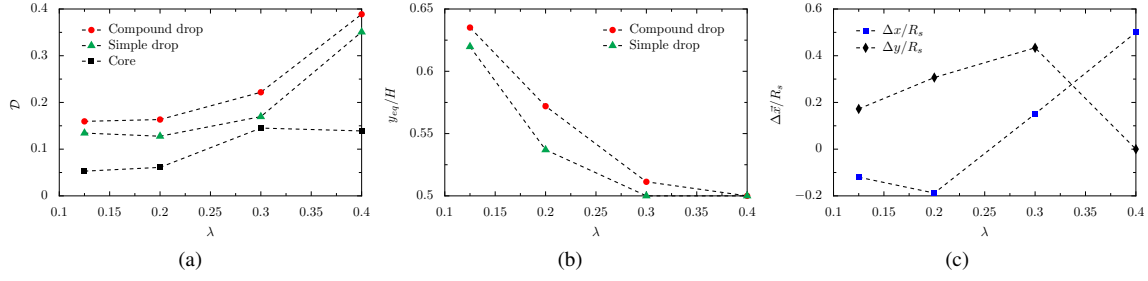


FIG. 10: Effect of aspect ratio on the (a) deformation of the compound drop and the core, (b) migration of the compound drop, and (c) eccentricity of the core at equilibrium. Other parameters were kept fixed at $K = 0.5$, $\mu_r = 1$ and $Ca = 1$.

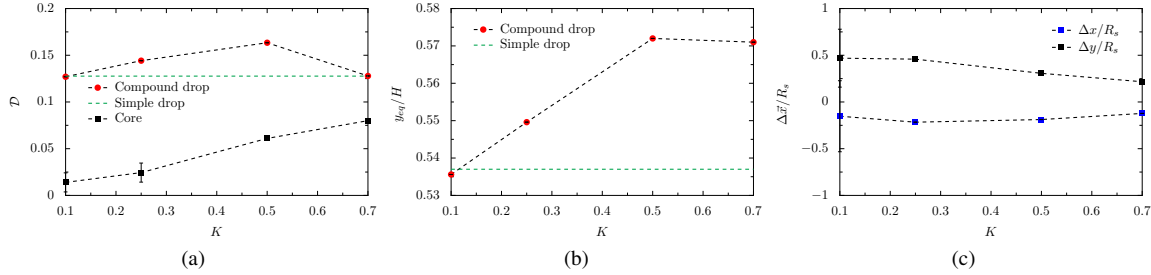


FIG. 11: Effect of radius ratio on the (a) deformation of the compound drop and the core, (b) migration of the compound drop, and (c) eccentricity of the core. Other parameters were kept fixed at $\lambda = 0.2$, $\mu_r = 1$ and $Ca = 1$.

the stable state is observed increases with decrease in radius ratio. This behavior is expected since smaller cores are able to resist deformation since they have larger capillary pressure.

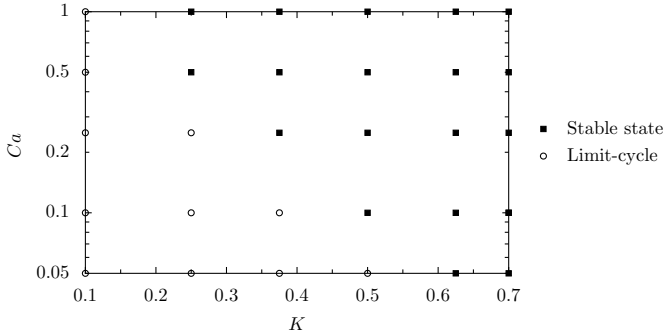


FIG. 12: Regime map showing the two equilibrium states in the (K, Ca) space. Other parameters were kept fixed at $\lambda = 0.2$ and $\mu_r = 1$.

IV. SUMMARY

We have investigated numerically the hydrodynamics of a compound drop suspended in a Poiseuille flow under Stokes regime. Our results show that the core and shell interact and influence each other through the liquid in the gap between them. From these interactions, we identify two distinct equilibrium core behaviors: stable state and limit-cycle. In

the stable state the core stops revolving and starts moving outward very slowly. The core in the limit-cycle state, continues to revolve at a constant rate and in nearly a fixed orbit. By comparing with the simple drop, we find that the core in these two states enhance the deformation of the compound drop and also affects its migration. The slow outward motion of the core in the stable state pushes the compound drop slightly towards the wall. The revolving core in the limit-cycle state makes the compound drop to oscillate as it migrates. We also find that the migration of the compound drop affects the eccentricity of the core.

We also conducted a parametric study to understand the influence of each parameter on the core-shell interaction. The key results are the following.

- Increasing any parameter results in the transition from limit-cycle state to stable state occurs. This transition occurs due to the increased deformation of the core.
- The deformation of the compound drop is enhanced only at intermediate core sizes. At extreme sizes, the deformation of the compound drop is nearly same as the simple drop. This behavior is due to either very less interaction at small core sizes or the increased interactions at large sizes.
- The migration of the compound drop moves increasingly towards the wall with increasing core size.
- Both the core and the shell become symmetric about the centerline only when the equilibrium position of the

compound drop is at the center. In this symmetric position, the core is still eccentric and occupies the front of the shell.

The similarities with the results reported in the literature shows that the essential physics of the compound drops in Poiseuille flows is captured sufficiently by our 2D simulations. We believe these results provide a better understanding of the compound drops in pressure-driven flows, which can be used to identify favorable flow conditions for various applications.

V. SUPPLEMENTARY MATERIAL

The supplementary material contains plots showing the effect of initial conditions such as the release height of the drop and the initial eccentricity on the migration and deformation dynamics of the core and the compound drop.

ACKNOWLEDGMENTS

V.T.G would like to acknowledge the financial support from IIT Madras via the institute post-doctoral fellowship. **V.T.G** is grateful for insightful discussions with Mr. Akash Choudary, Mr. K.V.S Chaithanya, and Mr. Prathamesh Makarant Vinze.

VI. DATA AVAILABILITY

The data that supports the findings of this study are available within the article and its supplementary material.

Appendix A: Grid independence study

In order to ensure that the parameters measured and the flow fields are resolved accurately, we have performed a grid convergence study. Since we use adaptive mesh refinement, we varied the maximum refinement levels from 8 to 10 in steps of one. So, the smallest mesh size of levels 8,9,10 are 3.9×10^{-3} , 1.9×10^{-3} , 9.8×10^{-4} respectively. It can be concluded from the FIG. 13 that variation in the measured parameters between different mesh sizes is minimal, so we use a maximum refinement of 9 levels for all our simulations.

Appendix B: Validation

We validated the solver used in our work with the experimental and numerical results reported in the literature^{34,49}. First we validate the solver with the results obtained from drops migrating in a capillary tube⁴⁹ at different capillary numbers. This problem is simulated under Stokes regime in axisymmetric configuration, and the computational setup is a rectangular domain of size 6×1 . The steady state shapes of the drop from the simulations are compared with the shapes

from the experiments in the FIG. 14, and we get an excellent match with the experiments.

We also verified our solver by simulating the migration of a small drop ($\lambda = 0.125$) in a plane Poiseuille flow³⁴ at different viscosity ratios. In this problem, we solve the full Navier-Stokes equations including the inertial terms in a square computational domain of size one. As shown in the FIG. 15, we get an excellent agreement with the reported results for the trajectory of the drop at different viscosity ratios.

- ¹T. Norimatsu, Y. Izawa, K. Mima, and P. M. Gresho, "Modeling of the centering force in a compound emulsion to make uniform plastic shells for laser fusion targets," *Fusion Technology* **35**, 147–156 (1999).
- ²M. Liu, L. Su, J. Li, S. Chen, Y. Liu, J. Li, B. Li, Y. Chen, and Z. Zhang, "Investigation of spherical and concentric mechanism of compound droplets," *Matter and Radiation at Extremes* **1**, 213–223 (2016).
- ³C. X. Zhao, "Multiphase flow microfluidics for the production of single or multiple emulsions for drug delivery," *Advanced Drug Delivery Reviews* **65**, 1420–1446 (2013).
- ⁴E. Dickinson, "Double Emulsions Stabilized by Food Biopolymers," *Food Biophysics* **6**, 1–11 (2011).
- ⁵A. G. Håti, N. B. Arnfinnsdottir, C. Østevold, M. Sletmoen, G. Etienne, E. Amstad, and B. T. Stokke, "Microarrays for the study of compartmentalized microorganisms in alginate microbeads and (W/O/W) double emulsions," *RSC Advances* **6**, 114830–114842 (2016).
- ⁶T. Alkayyali, T. Cameron, B. Haltli, R. G. Kerr, and A. Ahmadi, "Microfluidic and cross-linking methods for encapsulation of living cells and bacteria - A review," *Analytica Chimica Acta* **1053**, 1–21 (2019).
- ⁷R. Johnson, "Fluid Mechanics of Compound Multiphase Drops and Bubbles," *Annual Review of Fluid Mechanics* **17**, 298–320 (1985).
- ⁸S. S. Sadhal and H. N. Oguz, "Stokes flow past compound multiphase drops: The case of completely engulfed drops/bubbles," *Journal of fluid Mechanics* **160**, 511–529 (1985).
- ⁹I. Bazhlekoy, P. J. Shopov, and Z. D. Zapryanov, "Unsteady motion of a type-A compound multiphase at moderate Reynolds numbers," *Journal of Colloid And Interface Science*, 1–12 (1995).
- ¹⁰S. Homma, M. Yokotsuka, T. Tanaka, K. Moriguchi, J. Koga, and G. Trygvason, "Numerical simulation of an axisymmetric compound droplet by three-fluid front-tracking method," *Fluid Dynamics and Materials Processing* **7**, 231–240 (2011).
- ¹¹L. L. G. Stone H.A., "Breakup of concentric double emulsions droplets in linear flows," *Journal of Fluid Mechanics* **211**, 123–156 (1990).
- ¹²J. Wang, X. Wang, M. Tai, and J. Guan, "Oriented shift and inverse of the daughter droplet due to the asymmetry of grand-daughter droplets of multiple emulsions in a symmetric flow field," *Applied Physics Letters* **108** (2016).
- ¹³J. Wang, S. Xu, Y. Huang, and J. Guan, "Mechanical mechanisms of the directional shift and inverse of the eccentric compound droplet," *Physics of Fluids* **30** (2018).
- ¹⁴K. A. Smith, J. M. Ottino, and M. O. De La Cruz, "Encapsulated drop breakup in shear flow," *Physical Review Letters* **93**, 1–4 (2004).
- ¹⁵X. Qu and Y. Wang, "Dynamics of concentric and eccentric compound droplets suspended in extensional flows," *Physics of Fluids* **24** (2012), 10.1063/1.4770294.
- ¹⁶H. Hua, J. Shin, and J. Kim, "Dynamics of a compound droplet in shear flow," *International Journal of Heat and Fluid Flow* **50**, 63–71 (2014).
- ¹⁷Y. Chen, X. Liu, C. Zhang, and Y. Zhao, "Enhancing and suppressing effects of an inner droplet on deformation of a double emulsion droplet under shear," *Lab on a Chip* **15**, 1255–1261 (2015).
- ¹⁸Y. Chen, X. Liu, and Y. Zhao, "Deformation dynamics of double emulsion droplet under shear," *Applied Physics Letters* **106** (2015).
- ¹⁹T. V. Vu, T. V. Vu, and D. T. Bui, "Numerical study of deformation and breakup of a multi-core compound droplet in simple shear flow," *International Journal of Heat and Mass Transfer* **131**, 1083–1094 (2019).
- ²⁰C. Zhou, P. Yue, and J. J. Feng, "Deformation of a compound drop through a contraction in a pressure-driven pipe flow," *International Journal of Multiphase Flow* **34**, 102–109 (2008).
- ²¹Y. Song, J. Xu, and Y. Yang, "Stokes flow past a compound drop in a circular tube," *Physics of Fluids* **22**, 1–19 (2010).

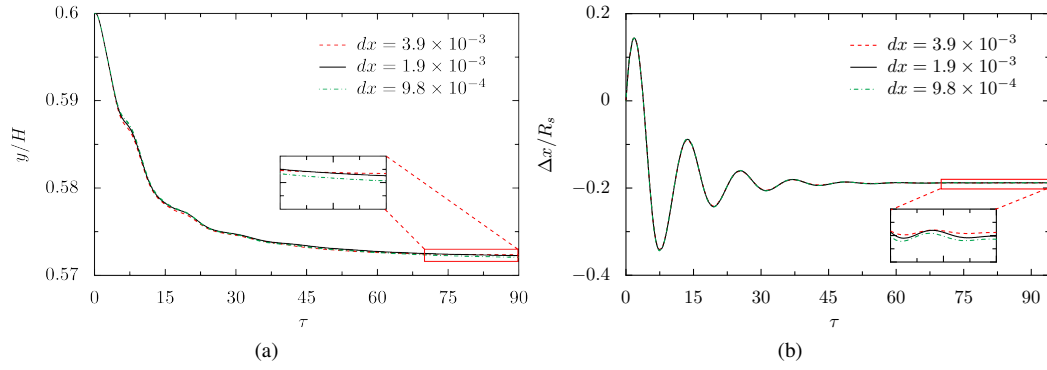


FIG. 13: Effect of mesh resolution on (a) trajectory of the compound drop and (b) eccentricity of the core. The parameters used for this simulation are $\lambda = 0.2$, $K = 0.5$, $\mu_r = 1$ and $Ca = 1$.

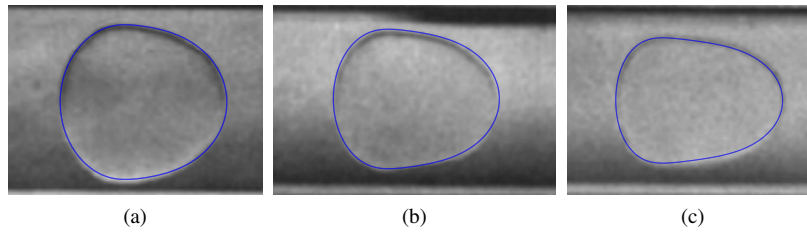


FIG. 14: Comparison of steady state drop shapes between the experiments⁴⁹ and the simulations (shown in blue lines) at (a) $Ca = 0.05$ (b) $Ca = 0.1$ (c) $Ca = 0.16$. Other parameters are $\mu_r = 1.05$ and $\lambda = 0.95$.

- ²²J. Tao, X. Song, J. Liu, and J. Wang, "Microfluidic rheology of the multiple-emulsion globule transiting in a contraction tube through a boundary element method," *Chemical Engineering Science* **97**, 328–336 (2013).
- ²³M. P. Borthakur, G. Biswas, and D. Bandyopadhyay, "Dynamics of deformation and pinch-off of a migrating compound droplet in a tube," *Physical Review E* **97**, 1–9 (2018).
- ²⁴Z. Che, Y. F. Yap, and T. Wang, "Flow structure of compound droplets moving in microchannels," *Physics of Fluids* **30** (2018).
- ²⁵S. Guido and V. Preziosi, "Droplet deformation under confined poiseuille flow," *Advances in Colloid and Interface Science* **161**, 89 – 101 (2010), physico-chemical and flow behaviour of droplet based systems.
- ²⁶J. M. Martel and M. Toner, "Inertial Focusing in Microfluidics," *Annual Review of Fluid Mechanics* **24** (2014).
- ²⁷C. Yu, L. Wu, L. Li, and M. Liu, "Experimental study of double emulsion formation behaviors in a one-step axisymmetric flow-focusing device," *Experimental Thermal and Fluid Science* **103**, 18–28 (2019).
- ²⁸J. Brackbill, D. Kothe, and C. Zemach, "A continuum method for modeling surface tension," *Journal of Computational Physics* **100**, 335 – 354 (1992).
- ²⁹S. Popinet, "Gerris: a tree-based adaptive solver for the incompressible euler equations in complex geometries," *Journal of Computational Physics* **190**, 572 – 600 (2003).
- ³⁰S. Popinet, "An accurate adaptive solver for surface-tension-driven interfacial flows," *Journal of Computational Physics* **228**, 5838 – 5866 (2009).
- ³¹J. B. Bell, P. Colella, and H. M. Glaz, "A second-order projection method for the incompressible navier-stokes equations," *Journal of Computational Physics* **85**, 257 – 283 (1989).
- ³²M. M. Francois, S. J. Cummins, E. D. Dendy, D. B. Kothe, J. M. Sicilian, and M. W. Williams, "A balanced-force algorithm for continuous and sharp interfacial surface tension models within a volume tracking framework," *Journal of Computational Physics* **213**, 141 – 173 (2006).
- ³³S. Afkhami and M. Bussmann, "Height functions for applying contact angles to 2d vof simulations," *International Journal for Numerical Methods in Fluids* **57**, 453–472 (2008).
- ³⁴S. Mortazavi and G. Tryggvason, "A numerical study of the motion of drops in Poiseuille flow. Part 1. Lateral migration of one drop," *Journal of Fluid Mechanics* **411**, 325–350 (2000).
- ³⁵C. A. Stan, L. Guglielmini, A. K. Ellerbee, D. Caviezel, H. A. Stone, and G. M. Whitesides, "Sheathless hydrodynamic positioning of buoyant drops and bubbles inside microchannels," *Physical Review E - Statistical, Nonlinear, and Soft Matter Physics* **84**, 1–19 (2011).
- ³⁶H. Lan and D. B. Khismatullin, "A numerical study of the lateral migration and deformation of drops and leukocytes in a rectangular microchannel," *International Journal of Multiphase Flow* **47**, 73–84 (2012).
- ³⁷G. I. Taylor, "The formation of emulsions in definable fields of flow," *Proceedings of the Royal Society of London. Series A. Containing Papers of a Mathematical and Physical Character* **146**, 501–523 (1934).
- ³⁸S. Kim and S. Dabiri, "Transient dynamics of eccentric double emulsion droplets in a simple shear flow," *Physical Review Fluids* **2**, 1–17 (2017).
- ³⁹"Reactions in double emulsions by flow-controlled coalescence of encapsulated drops," *Lab on a Chip* **11**, 2312–2315 (2011).
- ⁴⁰M. D. Graham, *Microhydrodynamics, Brownian Motion, and Complex Fluids*, Cambridge Texts in Applied Mathematics (Cambridge University Press, 2018).
- ⁴¹Y. N. Young, J. Bławdziewicz, V. Cristini, and R. H. Goodman, "Hysteretic and chaotic dynamics of viscous drops in creeping flows with rotation," *Journal of Fluid Mechanics* **607**, 209–234 (2008).
- ⁴²J. Bławdziewicz, R. H. Goodman, N. Khurana, E. Wajnryb, and Y. N. Young, "Nonlinear hydrodynamic phenomena in Stokes flow regime," *Physica D: Nonlinear Phenomena* **239**, 1214–1224 (2010).
- ⁴³P. C. Chan and L. G. Leal, "The motion of a deformable drop in a second-order fluid," *Journal of Fluid Mechanics* **92**, 131–170 (1979).
- ⁴⁴S. C. Hur, N. K. Henderson-Maclennan, E. R. McCabe, and D. Di Carlo, "Deformability-based cell classification and enrichment using inertial microfluidics," *Lab on a Chip* **11**, 912–920 (2011).
- ⁴⁵B. V. Hokmabad, K. A. Baldwin, C. Krüger, C. Bahr, and C. C. Maass, "Topological Stabilization and Dynamics of Self-propelling Nematic Shells," *Physical Review Letters* **123**, 178003 (2018), arXiv:1810.07223.
- ⁴⁶S. Okushima, T. Nisisako, T. Torii, and T. Higuchi, "Controlled production

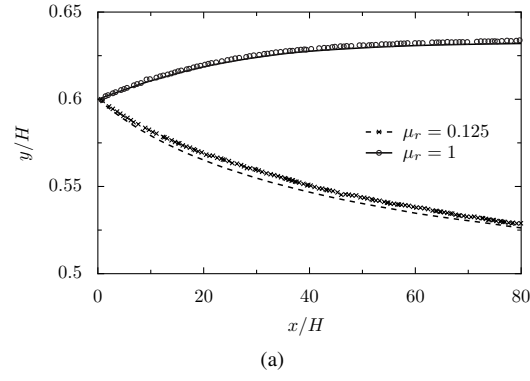


FIG. 15: Trajectory of the drop at $Re(=U_m H/\nu_c) = 1$, $Ca = 0.25$, $\lambda = 0.125$. The lines represent current simulation and the markers represent the simulation data from³⁴.

of monodisperse double emulsions by two-step droplet breakup in microfluidic devices,” *Langmuir* **20**, 9905–9908 (2004).

⁴⁷E. W. Kemna, R. M. Schoeman, F. Wolbers, I. Vermes, D. A. Weitz, and A. Van Den Berg, “High-yield cell ordering and deterministic cell-in-droplet encapsulation using Dean flow in a curved microchannel,” *Lab on a Chip* **12**, 2881–2887 (2012).

⁴⁸Z. Y. Luo, L. He, and B. F. Bai, “Deformation of spherical compound capsules in simple shear flow,” *Journal of Fluid Mechanics* **775**, 77–104 (2015).

⁴⁹W. L. Olbricht and D. M. Kung, “The deformation and breakup of liquid drops in low reynolds number flow through a capillary,” *Physics of Fluids A: Fluid Dynamics* **4**, 1347–1354 (1992).